A nano-patterned photonic crystal laser with a dye-doped liquid crystal

AIP | Applied Physics Letters

A nano-patterned photonic crystal laser with a dye-doped liquid crystal

Doo-Hyun Ko, Stephen M. Morris, Alexander Lorenz, Flynn Castles, Haider Butt et al.

Citation: Appl. Phys. Lett. **103**, 051101 (2013); doi: 10.1063/1.4816243
View online: http://dx.doi.org/10.1063/1.4816243
View Table of Contents: http://apl.aip.org/resource/1/APPLAB/v103/i5
Published by the AIP Publishing LLC.

A nano-patterned photonic crystal laser with a dye-doped liquid crystal

Doo-Hyun Ko,[1,a)] Stephen M. Morris,[2,b)] Alexander Lorenz,[2] Flynn Castles,[2] Haider Butt,[2] Damian J. Gardiner,[2] Malik M. Qasim,[2] Bodo Wallikewitz,[1] Philip J. W. Hands,[2] Timothy D. Wilkinson,[2] Gehan A. J. Amaratunga,[2] Harry J. Coles,[2] and Richard H. Friend[1,c)]
[1]*Cavendish Laboratory, University of Cambridge, JJ Thomson Avenue, Cambridge CB3 0HE, United Kingdom*
[2]*Department of Engineering, University of Cambridge, 9 JJ Thomson Avenue, Cambridge CB3 0FA, United Kingdom*

(Received 10 April 2013; accepted 4 June 2013; published online 29 July 2013)

Covering a nano-patterned titanium dioxide photonic crystal (PC) within a well-oriented film of dye-doped liquid crystal (LC), a distributed feedback laser is constructed whereby the emission characteristics can be manipulated *in-situ* using an electric field. This hybrid organic-inorganic structure permits simultaneous selectivity of both the beam pattern and laser wavelength by electrical addressing of the LC director. In addition, laser emission is obtained both in the plane and normal to the PC. Along with experimental data, a theoretical model is presented that is based upon an approximate calculation of the band structure of this birefringent, tuneable laser device. © *2013 AIP Publishing LLC*. [http://dx.doi.org/10.1063/1.4816243]

Laser devices formed from two dimensional photonic crystals (PCs), based upon both inorganic[1–5] and organic[6–8] materials, have been fabricated demonstrating a range of remarkable emission properties.[9–11] Control of the laser emission characteristics can be achieved at the fabrication stage by pre-selecting the periodicity and the geometrical arrangement of the lattice. However, many potential applications of PC lasers would benefit from *in-situ* control of the emission properties. Tuneability can be achieved by infiltrating liquid crystals (LCs) into PCs so as to vary the spectral position of the photonic band gap through a range of external stimuli.[12–23] However, it is often difficult to align the LC uniformly in the zero-field state resulting in limited tuning capabilities.[20,21]

In this letter, we report on a compact laser that consists of a nano-patterned structure. A thin, nano-patterned titanium dioxide (TiO_2) layer is covered with a nematic, dye doped LC. Uniform alignment of the LC director is provided by gentle rubbing of the TiO_2-layer and by covering the device with a glass plate coated with both polyimide (PI) and indium tin oxide (ITO). With the rubbing directions of the PI and the TiO_2 layers being parallel, a uniform director field parallel to the *x*-*y*-plane (Figure 1) is created. The device shows distributed feedback lasing that can be characterized by the band structure of the thin PC layer, even though the PC layer possesses a finite thickness (expansion in *z*-direction) even smaller than the laser wavelength.[24] Additionally, the emission characteristics of the device can be manipulated *in-situ* by using a quasi static electric field that can be applied across the device. Above a threshold of $\approx 0.5\,V/\mu m$, the electric field induces realignment of the LC director parallel to the electric field lines.[25] By addressing the LC with an electric field, both the beam pattern and laser wavelength can be controlled simultaneously.

The TiO_2 nano-pattern was fabricated by embossing a TiO_2 sol-gel with a perfluoropolyether mould at 150 °C for 2 h under pressure.[26,27] After peeling off the mould, the TiO_2 film was then annealed at 450 °C for 2 h to increase the refractive index of the nano-patterned film. Measurement of the refractive index of flat TiO_2 layers fabricated with this method yielded values of ≈1.8 before and ≈2.0 after annealing, respectively, at a wavelength of 589 nm. As the active medium, a nematic LC[25] (E49, Merck KGaA) doped with 1 wt. % laser dye (4-(Dicyanomethylene)-2-methyl-6-(4-dimethylaminostyryl)-4H-pyran, Exciton) was used. The refractive indices of this mixture were found to be $n_e = 1.77$ and $n_o = 1.53$. As shown by scanning electron microscope images (Figure 1), the PC consisted of a hexagonal array of pillars with a protrusion of 130 nm, a pitch of $a = 400$ nm, and a radius of $r = 0.80\,nm = 0.2a$.

The LC alignment was investigated with polarized optical microscopy. Although the feature size of the nano-patterned TiO_2 layer is beyond the optical resolution, a non-uniform alignment at the TiO_2-LC interface would lead to intensity variations in the microscope field of view. In contrast, a defect free, uniform field of view was observed. Thus, a uniform alignment of the confined nematic LC can be

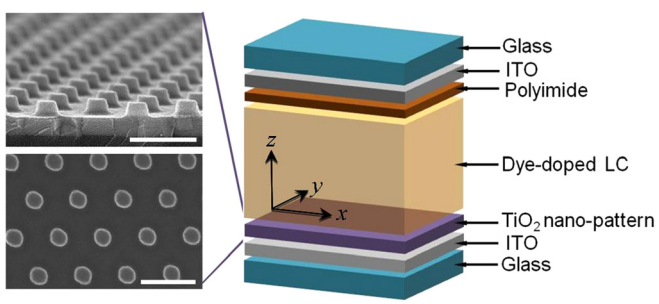

FIG. 1. SEM images of the PC layer and schematic of the TiO_2 PC/LC laser device. The SEM images show the cross-section and top view of the PC layer. All scale bars are 500 nm. Transparent electrodes on both the top and bottom substrates enabled an electrical field to be applied perpendicular to the plane of the PC.

[a)]Center for Opto-Electronic Convergence Systems, Korea Institute of Science and Technology, Seoul, Republic of Korea.
[b)]E-mail: smm56@cam.ac.uk
[c)]E-mail: rhf10@cam.ac.uk

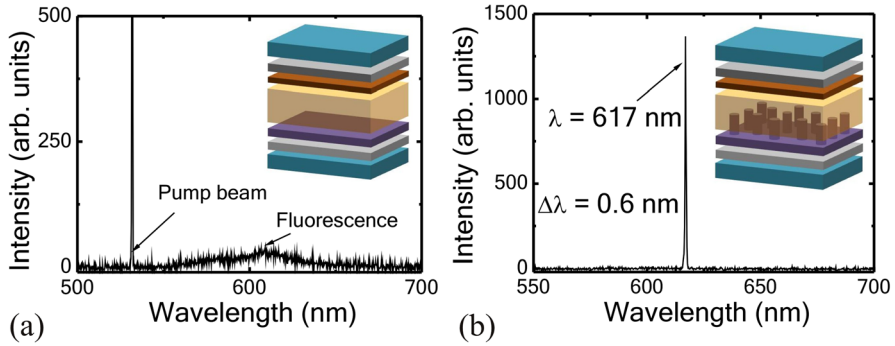

FIG. 2. Comparison of non-patterned and nano-patterned TiO_2-LC devices. (a) Fluorescence from the non-patterned TiO_2 device when photo-excited along a direction normal to the plane of the device. (b) Laser emission from the nano-patterned TiO_2-LC device. $\Delta\lambda$ represents the full-width at half maximum. The cell gap in both cases was 10 μm. The insets of the figures represent the two different device structures. Note that in (b) the height of the pillars is not to scale and is simply to indicate the nano-patterned array.

assumed. The thickness of the LC layer was defined to be 10 μm using spacer beads, which was chosen to ensure a large dye reservoir above the nano-patterned layer that could be replenished through thermal diffusion.

To confirm that distributed feedback of the thin PC-layer was responsible for the laser emission rather than leaky modes from within either the dye-doped nematic layer[28] or random amplification as a result of multiple scattering,[29,30] a device with a non-patterned TiO_2 layer was also studied. The TiO_2-LC samples were excited normal to the glass substrates by the second harmonic of an Nd:YAG laser (Polaris II, New Wave Research) at an excitation rate of 1 Hz and pulse width of 3–4 ns. The pump beam was focused to a spot of 100 μm. Emission was collected along the normal to the substrates for the 1st-order Bragg mode (surface emission) by a high numerical aperture objective and focused into an optical fiber that was connected to a broadband spectrometer with a resolution of 0.3 nm. In the device with the non-patterned TiO_2 layer, fluorescence but not lasing was observed (Figure 2(a)). For all excitation energies used, the threshold for amplified spontaneous emission was found to be greater than 10 000 nJ/pulse (130 mJ/cm^2). On the contrary, a thin PC layer provides distributed feedback at certain locations in the band structure where three dimensional lasing can be expected at specific points of the Brillouin-zone boundary corresponding to where the bands cross and split.[24] In the nano-patterned device, laser emission at a wavelength of 617 nm with a linewidth of 0.6 nm was observed (Figure 2(b)).

Incorporating the dye-doped LC film leads to the device becoming sensitive to the plane of polarization of the input beam. A half-wave plate was used to control the orientation of the plane of linear polarization relative to the LC director. Results for the input-output characteristics for two orthogonal polarizations are presented in Figure 3, which shows a notable change in the excitation threshold from $E_{th} = 89 \pm 5$ nJ/pulse (1.1 mJ/cm^2) to $E_{th} = 299 \pm 15$ nJ/pulse (3.8 mJ/cm^2). The large difference in the threshold is considered to be due to the change in the absorption of the dye through the dye-guest host effect;[29] the orientation of the transition dipole moment of the dye aligns preferentially with the director of the LC and therefore the absorption is maximized when the input polarization was parallel to the director.

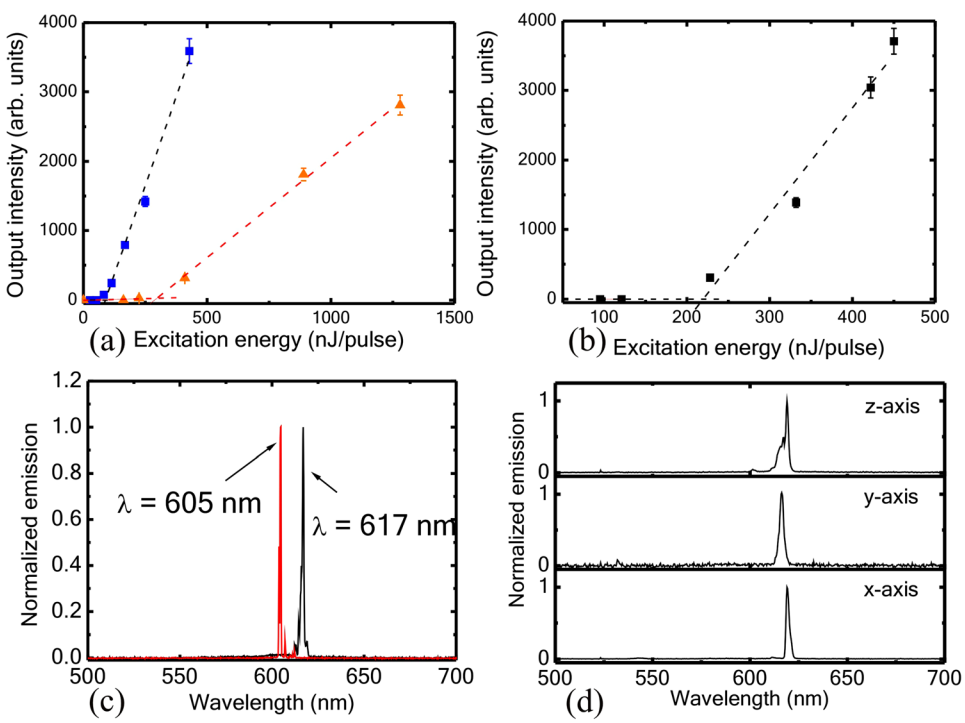

FIG. 3. Emission characteristics of the nano-patterned TiO_2-LC laser device. (a) The output intensity as a function of excitation energy for the two orthogonal linear polarization states of the TiO_2-LC laser when photo-excited normal to the plane of the device: parallel to the LC director (blue squares) and perpendicular to the director (orange triangles). (b) Output as a function of excitation energy for a chiral nematic LC laser with the same film thickness and dye. (c) Laser emission in the no-field state (black line) and with an applied electric field (5 kHz) with a field strength of 12 V/μm (red line). (d) Laser emission in three dimensions consisting of in-plane (x, y) and surface (z) emission.

The lowest recorded laser threshold for this device compares favourably with values that have been reported recently for other 2D surface-emitting PC lasers.[5] For comparison, the input-output curve of a conventional dye-doped chiral nematic LC that has a 1D periodic structure is shown in Figure 3(b), where the periodicity is perpendicular to the plane of the device. The 1D chiral nematic laser consisted of the same laser dye and nematic host as that of the TiO_2-LC laser. Furthermore, to ensure optimum conditions, the laser wavelength was matched to the gain maximum of the dye. For all factors being equal, there is almost a 3-fold decrease in the threshold for the nano-patterned TiO_2-LC laser as compared with the conventional chiral nematic LC laser.

Wavelength tuning of the TiO_2-LC laser device is shown in Figure 3(c) where it is observed that the emission wavelength can be blue-shifted by 12 nm and was found to be fully reversible. Upon removal of the applied electric field, the laser emission red-shifted back to the initial wavelength of 617 nm. The recovery of the initial wavelength was found to occur within the timescale set by the repetition rate of the pump laser (i.e., 1 s). The shift that is recorded here is larger than those observed previously in LC-infiltrated PC laser devices.[20] At the boundaries to the glass cover plate and the nano-patterned TiO_2, a finite coherence length of the elastic deformation of the LC may still be present. However, this coherence length decreases with the electric field strength. Therefore, a uniform director field where the LC director is parallel to the z-direction can be assumed to be in the field-on state, which was confirmed using polarizing optical microscopy. In addition to the laser emission in the z-direction, laser emission was also detected in the x-, y-direction (Figure 3(d)), as expected. The present experiments indicate that addressing of the LC with an electric field causes a shift of the laser wavelength of the three dimensional emission.

There is also a simultaneous change in the far-field beam profile from an elliptical shape to a circular profile when an electric field is applied, Figure 4. The far-field pattern is determined by the Fourier transform of the internal electromagnetic field distribution, which can be controlled by changing the refractive index profile of the medium between the pillars by adjusting the alignment of the LC. The change from an asymmetric to symmetric beam shape reflects the variation from an anisotropic refractive index profile within the plane of the pillars to a single refractive index value when the electric field is applied. Adjusting the polarization of the pump beam does not alter the far-field emission profile for both cases. The control of the beam profile using this configuration is an important development as it is generally only achievable through the appropriate design of the unit cell of the PC.[10]

The band structure of layered structures with a central, thin PC layer can be simulated in a two-stepped approach[24] where first, the fundamental mode of the layered structure is simulated and the effective refractive index n_{eff} and a confinement factor f_c in the PC layer are then extracted. Subsequently, the band diagram of a two-dimensional PC with infinite expansion in the z-direction, but with unchanged two-dimensional geometry ($p = 400$ nm, $r = 0.2p$) is calculated. To account for the finite thickness of the PC-layer, effective material constants are considered in this second step. An effective average dielectric constant $\bar{\varepsilon}$ is approximated as

$$\bar{\varepsilon} = n_{eff}^2 = \frac{\varepsilon_a + \varepsilon_b}{2}. \quad (1)$$

The effective dielectric contrast $\Delta\varepsilon$ and the effective dielectric constants ε_a (effective background material) and ε_b (in z-direction infinitely expanded cylinders) are calculated by using f_c and the dielectric constants of the background material ε_1 and of the pillars ε_2

$$\Delta\varepsilon = \varepsilon_b - \varepsilon_a = f_c \cdot (\varepsilon_2 - \varepsilon_1). \quad (2)$$

First, a modal analysis of a cross section of the structure along the Γ-J-direction was conducted by using a full vectorial finite element method-based algorithm (COMSOL

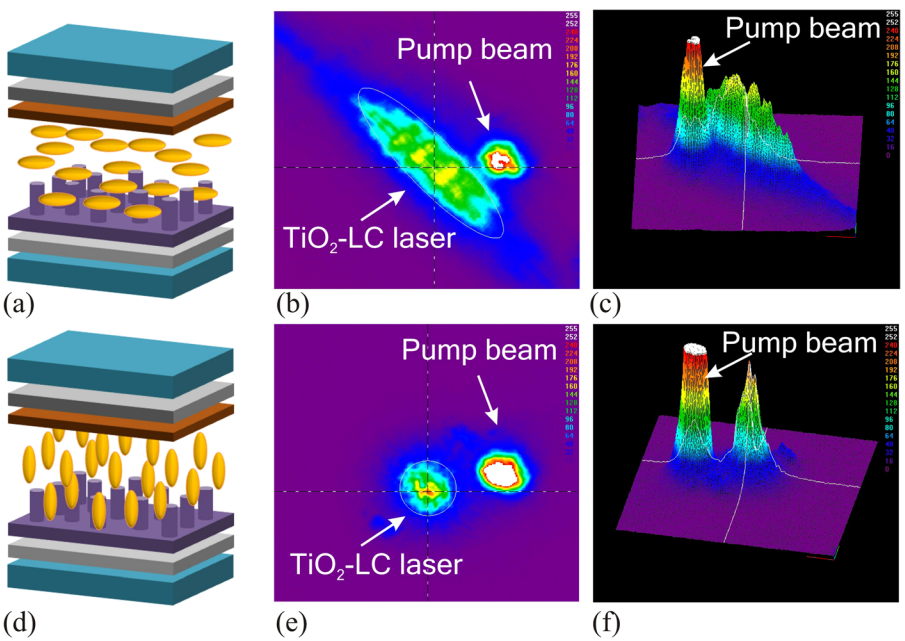

FIG. 4. Modification of the far-field beam profile using electric fields. No electric field: (a) illustration of the LC alignment, (b) 2D plot of the beam profile, and (c) 3D plot of the beam profile. (d), (e), and (f) are equivalent figures when the sample is subjected to an electric field (12 V/μm at 5 kHz). These results were recorded on a Spiricon Beam Profiler.

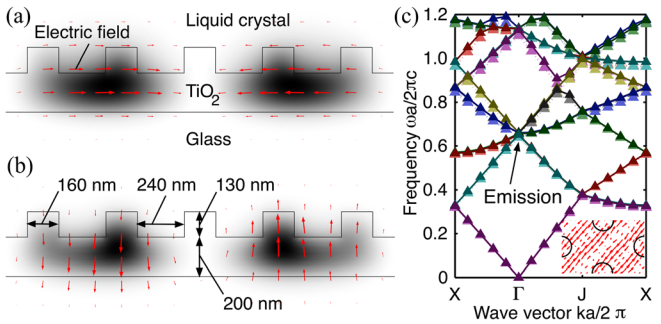

FIG. 5. (a) and (b) Two dimensional modal analysis of a cross section of the laser device where the LC filled region is modelled as an optical uniaxial medium with optic axis parallel to the *x*-direction. Two modes with comparable symmetry are shown: (a) *x*-polarized mode, (b) *z*-polarized mode. ((c) light colored symbols) Band diagram obtained for the case that the LC was considered as uniaxial with optic axis parallel to the *x*-direction, ((c) dark colored symbols) band diagram obtained for the case that the LC was considered as uniaxial with optic axis parallel to the *z*-direction. ((c) inset) Electric field distribution of a selected transverse electric mode (linearly polarized) of the simulated, planar photonic crystal. For the purposes of the simulation, the region below the nano-pillars was considered to be 200 nm-thick with an effective refractive index of 2.0. In the experiment, this layer would consist of both TiO_2 and ITO.

Multiphysics, version 4.3a). Periodic boundary conditions were applied at the boundaries parallel to the *z*-direction. Dielectric constants of 1.46^2 and of 2.0^2 were considered for the glass and for the TiO_2, respectively. The simulated wavelength was 589 nm. In the LC filled region, a uniaxial diagonal dielectric tensor was considered with the elements $\varepsilon_{xx} = n_e^2$ and $\varepsilon_{yy} = \varepsilon_{zz} = n_o^2$, in order to model the birefringence of the LC.

Two modes of low order and comparable symmetry were investigated in more detail; one was *x*-polarized (Figure 5(a)) and the other was *z*-polarized (Figure 5(b)). These modes were confined in the nano-patterned TiO_2 layer due to total internal reflection. The modal confinement factors of both modes were extracted as a ratio of the integral of the normalized electric fields in the 130 nm-thick PC layer and the integral of the normalized electric field in the entire simulation area.[26] Each mode possessed a confinement factor of $f_c \approx 23\%$. Since the two modes were polarized either parallel or perpendicular to the optic axis of the LC, one value of $\Delta\varepsilon$ was calculated, respectively, by inserting either $\varepsilon_1 = n_e^2$ (*x*-polarized mode) or $\varepsilon_1 = n_o^2$ (*z*-polarized mode) in Eq. (2). The results are listed in Table I. As expected, the calculated value of $\Delta\varepsilon_x$ (*x*-polarized mode) is smaller than the calculated value $\Delta\varepsilon_z$ (*z*-polarized mode). An effective dielectric constant of the infinitely extended cylinders ($\varepsilon_b = 3.616$) was approximated from $\bar{\varepsilon}$ obtained for the *x*-polarized mode because it is a close approximation of the fundamental mode.

TABLE I. Polarization and dielectric properties of two simulated modes of a two dimensional cross section of the layered structure with nano-patterned TiO_2 layer covered by a birefringent LC.

Director field	Polarization	ε_1	ε_2	$\bar{\varepsilon}$	$\Delta\varepsilon$
Uniaxial x	*X*	n_e^2	2.0^2	3.415	$\Delta\varepsilon_x = 0.403$
Uniaxial x	*Z*	n_o^2	2.0^2	3.152	$\Delta\varepsilon_z = 0.581$
Uniaxial z	*X*	n_o^2	2.0^2	3.301	$\Delta\varepsilon_x = 0.516$
Uniaxial z	*Z*	n_e^2	2.0^2	3.171	$\Delta\varepsilon_z = 0.407$

The band diagram was calculated with MIT photonic bands (MPB),[30] where a diagonal dielectric tensor ($\varepsilon_{xx} = \varepsilon_b - \Delta\varepsilon_x$ and $\varepsilon_{yy} = \varepsilon_{zz} = \varepsilon_b - \Delta\varepsilon_z$) was considered to model the birefringent background material (uniaxial with optic axis along the Γ-J-direction). The calculated band diagram is shown (Fig. 5(c), light colored symbols). A point of the Brillouin-zone boundary where six bands couple is indicated by an arrow. Laser emission perpendicular to the layers of the structure can be expected at this point.[24] Accordingly, the simulation results in six possible laser modes at wavelengths of $\approx 618 \pm 8$ nm, which is in good agreement with the experiments, where lasing at a wavelength of 617 nm was observed. The simulation was repeated by considering a birefringent medium with optic axis parallel to the *z*-direction to model the case that the LC director was uniformly aligned with the application of an electric field. The simulation resulted in modes with varying confinement factors (20.6% for the *x*-polarized mode and 23.9% for the *z*-polarized mode). From the dielectric data (Table I), values were obtained for use in the diagonal dielectric tensor ($\varepsilon_{xx} = \varepsilon_{yy} = \varepsilon_b - \Delta\varepsilon_x$ and $\varepsilon_{zz} = \varepsilon_b - \Delta\varepsilon_z$, with $\varepsilon_b = 3.56$) that was considered for the background material in the band diagram calculation. The result is shown (Figure 5(c), dark colored symbols). Additionally, one mode with linear polarization of the electric field is shown [Fig. 5(c), inset]. This mode is blue shifted from 620 nm (first simulation) to 607 nm (second simulation). A blue-shift ranging from 4 to 14 nm in magnitude was predicted for all simulated modes, respectively. The presented model cannot predict the exact behaviour of the real device, since it is only two-dimensional[24] and alignment effects of the LC cannot be considered. Nevertheless, it is in good qualitative agreement with the experiments.

In summary, these results demonstrate a laser device that has the capacity to "tune on demand" a number of emission properties besides the laser wavelength. This is in contrast to the tuning method of passive systems which involve a "tuning by design" approach to change factors such as the lattice constant, filling fraction, and symmetry of the PC. The presented results are encouraging for the fabrication of distributed feedback lasers using thin PC layers and other LC phases, which may result in alternative beam profiles providing a greater variety. Further work on the role of the device thickness on the performance of the laser would also be of interest.

The authors gratefully acknowledge the financial support of the Engineering and Physical Sciences Research Council (UK) through the COSMOS Technology Translation award (EP/H046658/1). One of the authors (S.M.M.) acknowledges The Royal Society for financial support and one of the authors (A.L.) acknowledges financial support by the German Research Council (DFG, LO 1922/1-1). Use of NCN/nanohub.org computational resources [MIT Photonic Bands, Ref. 30] is gratefully acknowledged.

[1]M. Imada, S. Noda, A. Chutinan, T. Tokuda, M. Murata, and G. Sasaki. Appl. Phys. Lett. **75**, 316 (1999).
[2]A. Mekis, M. Meier, A. Dodabalapur, R. E. Slusher, and J. D. Joannopoulos, Appl. Phys. A **69**, 111 (1999).

[3]K. Inoue, M. Sasada, J. Kawamata, K. Sakoda, and J. W. Haus, Jpn. J. Appl. Phys., Part 2 **38**, L157 (1999).
[4]D. Ohnishi, T. Okano, M. Imada, and S. Noda, Opt. Express **12**, 1562 (2004).
[5]T.-C. Lu, S.-W. Chen, L.-F. Lin, K. Tsung-Ting, C. C. Kao, P. Yu, H.-C. Kuo, S.-C. Wang, and S. Fan, Appl. Phys. Lett. **92**, 011129 (2008).
[6]M. Meier, A. Mekis, A. Dodabalapur, A. Timko, R. E. Slusher, J. D. Joannopoulos, and O. Nalamasu, Appl. Phys. Lett. **74**, 7 (1999).
[7]M. Meier, A. Dodabalapur, J. A. Rogers, R. E. Slusher, A. Mekis, A. Timko, C. A. Murray, R. Ruel, and O. Nalamasu, J. Appl. Phys. **86**, 3502 (1999).
[8]M. Notomi, H. Suzuki, and T. Tamamura, Appl. Phys. Lett. **78**, 1325 (2001).
[9]S. Noda, M. Yokoyama, M. Imada, A. Chutinan, and M. Mochizuki, Science **293**, 1123 (2001).
[10]E. Miyai, K. Sakai, T. Okano, W. Kunishi, D. Ohnishi, and S. Noda, Nature **441**, 946 (2006).
[11]M. Yokoyama and S. Noda, IEEE J. Quantum Electron. **39**, 1074 (2003).
[12]S. W. Leonard, J. P. Mondia, H. M. van Driel, O. Toader, S. John, K. Busch, A. Birner, U. Gosele, and V. Lehmann, Phys. Rev. B **61**, R2389 (2000).
[13]D. M. Pustai, A. Sharkawy, S. Shi, and D. W. Prather, Appl. Opt. **41**, 5574 (2002).
[14]K. Busch and S. John, Phys. Rev. Lett. **83**, 967 (1999).
[15]K. Yoshino, Y. Shimoda, Y. Kawagishi, K. Nakayama, and M. Ozaki, Appl. Phys. Lett. **75**, 932 (1999).
[16]Q.-B. Meng, C.-H. Fu, S. Hayami, Z.-Z. Gu, O. Sato, and A. Fujishima, J. Appl. Phys. **89**, 5794 (2001).
[17]G. Mertens, T. Roder, R. Schweins, K. Huber, and H.-S. Kitzerow, Appl. Phys. Lett. **80**, 1885 (2002).
[18]H. Takeda and K. Yoshino, J. Appl. Phys. **92**, 5658 (2002).
[19]M. Ozaki, Y. Shimoda, M. Kasano, and K. Yoshino, Adv. Mater. **14**, 514 (2002).
[20]B. Maune, M. Loncar, J. Witzens, M. Hochberg, T. Baehr-Jones, D. Psaltis, A. Scherer, and Y. Qiu, Appl. Phys. Lett. **85**, 360 (2004).
[21]D. Kang, J. E. Maclennan, N. A. Clark, A. A. Zakhidov, and R. H. Baughman, Phys. Rev. Lett. **86**, 4052 (2001).
[22]H.-S. Kitzerow, A. Lorenz, and H. Matthias, Phys. Status Solidi A **204**, 3754 (2007).
[23]A. Lorenz and H.-S. Kitzerow, Appl. Phys Lett. **98**, 241106 (2011).
[24]M. Imada, A. Chutinan, S. Noda, and M. Mochizuki, Phys. Rev. B. **65**, 195306 (2002).
[25]P. G. de Gennes and J. Prost, *The Physics of Liquid Crystals* (Oxford University Press, Oxford, UK, 1995).
[26]D.-H. Ko, J. R. Tumbleston, W. Schenck, R. Lopez, and E. T. Samulski, J. Phys. Chem. C **115**, 4247 (2011).
[27]T. T. Truong, R. Lin, S. Jeon, H. H. Lee, J. Maria, A. Gaur, F. Hua, I. Meinel, and J. A. Rogers, Langmuir **23**, 2898 (2007).
[28]L. M. Blinov, G. Cipparrone, P. Pagliusi, V. V. Lazarev, and S. P. Palto Appl. Phys. Lett. **89**, 031114 (2006).
[29]G. Strangi, S. Ferjani, V. Barna, A. De Luca, C. Versace, N. Scaramuzza, and R. Bartolino, Opt. Express **14**, 7737 (2006).
[30]S. G. Johnson and J. D. Joannopoulos, Opt. Express **8**, 173 (2001).